ChemComm

COMMUNICATION

View Article Online
View Journal | View Issue

Cite this: *Chem. Commun.*, 2025, **61**, 1609

Received 27th November 2024,
Accepted 12th December 2024

DOI: 10.1039/d4cc06234e

rsc.li/chemcomm

Growth window optimization for large-size quasi-two-dimensional Dion–Jacobson type perovskites†

Yinghao Fan,[a] Hang Yin,[b] Xinyi Li,[a] Jiafu Yu,[a] Yue Hu,[c] Yuting Gao*[a] and Guangda Niu*[b]

Quasi-2D DJ type perovskites theoretically offer excellent properties for X-ray detection, but they often face issues such as phase segregation and small crystal size. In this study, we synthesized large single crystals of quasi-2D DJ type perovskite (3AMPY)(MA)Pb_2Br_7 using temperature-controlled crystallization. The resulting X-ray detector exhibited high resistivity (1.78×10^9 Ω cm), a carrier mobility–lifetime ($\mu\tau$) product of 9.32×10^{-4} cm^2 V^{-1}, a dark current of 5.6×10^{-8} A cm^{-2} V^{-1}, and a sensitivity of 129.86 μC Gy^{-1} cm^{-2}. These results demonstrate the potential of quasi-2D DJ type perovskites for high-performance X-ray detection and provide insights into improving crystal growth for optoelectronic applications.

X-ray detection is crucial in diverse fields such as medical diagnostics, industrial non-destructive testing, and security inspections.[1,2] The key parameters affecting detection performance include sensitivity and dark current.[3–6] Recently, lead halide perovskite materials have emerged as promising candidates for direct X-ray detection due to their high X-ray absorption efficiency, considerable carrier mobility–lifetime product, and high sensitivity.[7–10] The sensitivity of three-dimensional perovskite-based X-ray detectors has been improved to over 50 000 μC Gy^{-1} cm^{-4}.[11] However, the inferior resistivity of these compounds results in a dark current that is much higher than what is required for front-end circuit integration. Additionally, the migratory behavior of ions within three-dimensional perovskites often leads to drifting in the current baseline, adversely impacting the detection limit.[12]

To this end, various zero-dimensional, one-dimensional and two-dimensional perovskites have been explored for X-ray detection.[13–15] For example, zero-dimensional $MA_3Bi_2I_9$ was assembled as an X-ray detector, delivering a dark current of 8 pA at 20 V, a high sensitivity of 1947 μC Gy^{-1} cm^{-2}, and a very low detection limit of 83 nGy s^{-1}.[16] DJ type two-dimensional perovskite (4-ABA)PbI_4 crystals were used for X-ray detection with a dark current of 2.36 pA at 10 V and a sensitivity of 572 μC Gy^{-1} cm^{-2} at a bias voltage of 50 V.[17] The detection limit has been decreased to below 5 nGy s^{-1} for low-dimensional perovskite detectors. Nevertheless, low-dimensional perovskites exhibit limited charge transport and thus inferior detection sensitivity.

Drawing from the lessons of perovskite solar cells, quasi-two-dimensional (quasi-2D) perovskites with increased quantum well thicknesses offer a compelling combination of high charge transport, high resistivity, and high stability.[18] These qualities position them as promising materials with substantial potential for optoelectronic applications. For example, Yalan Zhang and Nam-Gyu Park used a quasi-two-dimensional perovskite, $GA(MA)_nPb_nI_{3n+1}$ (n = 5), as a light absorber for perovskite solar cells with a PCE of 22.26%.[19] However, a significant problem for applying quasi-2D perovskites is the difficulty in achieving pure phase and large-size crystal. Most previous studies include a wide distribution of quantum well thickness in their films, and the size of the crystals grown in the few available reports is only 6–100 mm^2.[20] Therefore, it is necessary to elucidate the mechanism for growing large-size quasi-2D perovskites and explore their potential properties for X-ray detection.

Herein, by optimizing the thermodynamics of chemical reactions and continuous adjustment of the temperature environment at different stages of the mixed reaction system, we have successfully regulated the degree of each reaction in the mixed system and the final reaction products obtained. We successfully synthesized pure phase single crystals of the quasi-2D DJ type perovskite (3AMPY)(MA)Pb_2Br_7 ("3AMPY" stands for

[a] *Engineering Research Center of Nano-Geomaterials of the Ministry of Education, Faculty of Materials Science and Chemistry, China University of Geosciences, Wuhan, 430074, China. E-mail: gaoyt@cug.edu.cn*
[b] *Wuhan National Laboratory for Optoelectronics and School of Optical and Electronic Information, Huazhong University of Science and Technology, Wuhan 430074, China. E-mail: guangda_niu@hust.edu.cn*
[c] *School of Chemistry, University of Edinburgh, Kings Buildings, Edinburgh EH9 3FJ, UK*

† Electronic supplementary information (ESI) available. See DOI: https://doi.org/10.1039/d4cc06234e

3-(aminomethyl)pyridine and "MA" for methylamine) by the method of temperature cooling crystallization (TCC).[21] The (3MPY)(MA)Pb_2Br_7 SC device displayed a high resistivity of 1.78×10^9 Ω cm and a $\mu\tau$ product of 9.32×10^{-4} cm^2 V^{-1}. As a result, the detector exhibited balanced detection performance (a dark current of 5.6×10^{-8} A cm^{-2} V^{-1} and a sensitivity of 129.86 μC Gy^{-1} cm^{-2}).

The general chemical framework for these perovskites was adjusted to $A'_mA_{n-1}M_nX_{3n+1}$, where A′ represents a large organic amino cation, A denotes a smaller cation, M signifies a metal cation with a high atomic number, X represents a halogen anion, and n indicates the number of inorganic layers situated between the elongated organic cations. When the number of inorganic layers between the large organic cations is one ($n = 1$), the resultant perovskite adopts a two-dimensional (2D) structure.[22] The preparation of ideal quasi-two-dimensional perovskite single crystals is quite challenging and is influenced by various factors, such as ambient temperature, the ion concentration ratio in the precursor solution, the temperature range for crystal growth, and the cooling rate.

To successfully produce a pure phase of quasi-two-dimensional perovskite, we combined the thermodynamic analysis of chemical reactions with experimental observations and iteratively adjusted the crystal growth process based on solubility curves, ultimately achieving the desired structure. As shown in Fig. 1(a and b), when MABr was added to the HBr solution containing dissolved lead bromide, a orange-red precipitate appeared immediately, which was confirmed to be $MAPbBr_3$ by XRD analysis. Similarly, the addition of 3AMPY to the same HBr solution resulted in the rapid formation of an light yellow precipitate, identified as $3AMPYPbBr_4$. When 3AMPY and MABr were both added to the HBr solution, the orange-red and light yellow precipitates were produced at the same time. Then we heated up the mixed system until the solute was fully dissolved. A gradual cooling of the solution led to the formation of solely yellow precipitates (Fig. 1(c)). The yellow precipitate was subsequently confirmed to be (3AMPY)(MA)Pb_2Br_7 by single-crystal XRD. From the chemical reaction point of view, the process involves three chemical reactions:

$$C_6H_8N_2\ (3AMPY) + PbBr_2 + 2HBr \rightarrow C_6H_{10}N_2PbBr_4\ (3AMPYPbBr_4) \quad (1)$$

$$CH_6NBr\ (MABr) + PbBr_2 \rightarrow CH_6NPbBr_3\ (MAPbBr_3) \quad (2)$$

$$C_6H_8N_2\ (3AMPY) + CH_6NBr\ (MABr) + 2PbBr_2 + 2HBr \rightarrow C_7H_{16}N_3Pb_2Br_7\ ((3AMPY)(MA)Pb_2Br_7) \quad (3)$$

Thus, it can be concluded that reactions (1) and (2) can occur spontaneously at room temperature, whereas reaction (3) cannot, indicating a high energy barrier for the reaction (3). By providing energy to the system at elevated temperatures, we supply the necessary energy for reaction (3) to overcome the reaction barrier, allowing it to occur dominantly at high temperatures. Furthermore, in the mixed precursor liquid system with a determined ratio, the product (3AMPY)(MA)Pb_2Br_7 has the lowest formation energy (Fig. 1(d)). This aligns with the experimental observation where, after warming to dissolve the precipitate and subsequently cooling down, only (3AMPY)(MA)Pb_2Br_7 could be obtained.

We further analyze the experimental phenomena arising from the mixed system from the point of view of macroscopic solubility. The solubility profiles of MA^+ and Pb^{2+} ions in the hydrobromic acid solvent system were measured. It was observed that the solubility of all three ions in hydrobromic acid increased gradually with increasing temperature; however, the changes varied significantly among the ions. Notably, the solubility of 3AMPY in HBr is exceedingly high. During the experiment, it was impractical to measure the curve of its solubility in pure solvent as a function of temperature. This limitation is likely due to the complete ionization of the reaction products of 3AMPY with HBr in the acid, which prevents the formation of stable bromine salts that could precipitate out. We found that the solubility curves of the two ions are closer to each other with respect to temperature in the mixed system with the ratio of $3AMPY^{2+}$ and MA^+ in the precursor solution set at 1 : 6. The ratio of the slopes of the solubility curves as a function of temperature is closer to 1 : 1 (Fig. 1(f)), and we believe that this is the macroscopic reason for obtaining quasi-two-dimensional perovskites with an n-value of 2. Moreover, we designed a temperature control program for the subsequent growth of large-size crystals from these two curves. The temperature range of the crystal growth phase was set at 40–50 °C because the slope ratio of the solubility curves of the two phases in this range is closest to 1. This is also to ensure that only pure quasi-2D perovskites with an n-value of 2 are present in the final material, and no other heterogeneous phases are present.

The large crystals of (3AMPY)(MA)Pb_2Br_7 were synthesized using the TCC method. Initially, the reactants were completely dissolved in HBr at elevated temperatures according to specific

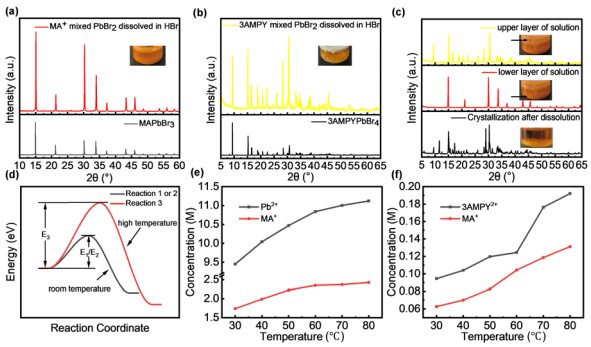

Fig. 1 (a) and (b) The XRD of the product addition of MA^+ and 3AMPY alone to a solution of dissolved $PbBr_2$ in HBr at room temperature. (c) The XRD of the products by sequential addition of MA^+ and 3AMPY to a solution of HBr with dissolved $PbBr_2$ at room temperature. (d) The schematic diagram of the chemical reaction potentials. (e) The solubility *versus* temperature graph of Pb^{2+} and MA^+ in hydrobromic acid. (f) The solubility *versus* temperature graph of $3AMPY^{2+}$ and MA^+ in the precursor solution.

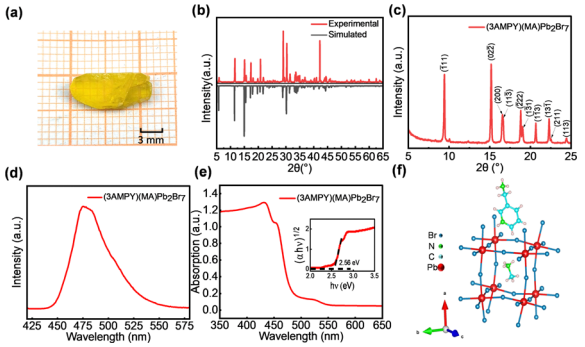

Fig. 2 The characterization of a (3AMPY)(MA)Pb_2Br_7 single crystal. (a) The photo of the crystal. (b) and (c) The powder XRD. (d) The photoluminescence spectra. (e) The UV-Vis diffuse reflectance spectra with band gap fitting. (f) The crystal structure of (3AMPY)(MA)Pb_2Br_7.

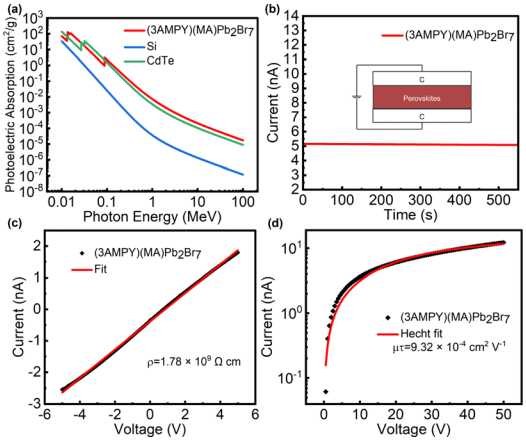

Fig. 3 (a) Absorption spectra of (3AMPY)(MA)Pb_2Br_7, Si, and CdTe as a function of X-ray photon energy. (b) Prepared device structure and dark current test results at 10 V. (c) *I*–*V* traces of the (3AMPY)(MA)Pb_2Br_7 detector in the dark. (d) The voltage-dependent photoconductivity of (3AMPY)(MA)Pb_2Br_7.

stoichiometric ratios until a clear and transparent solution was achieved. Subsequently, the solution was gradually cooled, allowing for crystal precipitation, which resulted in the acquisition of crystals as depicted in Fig. 2(a). Through various methods, we finally obtained a single crystal with a size of about 10 mm × 5 mm × 4 mm. To analyze the phase composition of the crystals, powder X-ray diffraction (XRD) was performed, and the results are presented in Fig. 2(b and c). The XRD patterns exhibited a close correspondence between the peak positions of both the experimental and simulated data, particularly in the low-angle region, indicating the successful synthesis of the two crystals with a high level of purity.

Subsequently, the photophysical properties of the crystals were characterized using photoluminescence (PL) spectroscopy and UV-visible absorption spectroscopy, as shown in Fig. 2(e and f). PL spectroscopy revealed a peak position at 475 nm (excitation wavelength of 390 nm) for the (3AMPY)(MA)Pb_2Br_7 crystals, with the fluorescence emission peak at 450 nm shifted by 20 nm toward longer wavelengths compared to the pure 2D perovskite 3AMPYPbBr_4. The UV-Vis spectroscopy analysis indicated an absorption edge at 479 nm for the crystal. Calculations based on these absorption edges yielded a band gap value of 2.56 eV for (3AMPY)(MA)Pb_2Br_7, which is smaller than that of the pure 2D perovskite 3AMPYPbBr_4 (2.78 eV) and larger than that of the 3D perovskite MAPbBr_3 (2.19 eV).[23] These results provide valuable insights into the optical properties and potential applications of these synthesized perovskite crystals in optoelectronic devices.

Single-crystal X-ray diffraction (XRD) analyses were conducted on (3AMPY)(MA)Pb_2Br_7 crystals, with the results displayed in Fig. 2(f). The findings revealed that (3AMPY)(MA)Pb_2Br_7 crystallizes in the $P2_1/c$ space group within the monoclinic crystal system (detailed test data in Table S1, ESI†). The crystal structure consists of lead bromide octahedra with interconnected vertices extending infinitely in the *b*–*c* plane, forming a two-dimensional inorganic perovskite layer. Additionally, the two inorganic layers are connected at the opposite ends of the $3AMPY^{2+}$ cation *via* robust N···H–Br hydrogen bonds, resulting in a quasi-two-dimensional perovskite structure where the organic and inorganic layers alternate along the *a*-axis.

The synthesized quasi-two-dimensional perovskite crystals were further investigated for X-ray detection due to their high atomic number (*Z*) elements, high mass stopping power (SC), and high resistivity. To assess the effectiveness of the crystals, the absorption spectra of several common materials (Si, CdTe) over a specific photon energy range were simulated based on the photon cross section database (in Fig. 3(a)). The absorption coefficients of the crystals are comparable to those of CdTe and higher than those of Si, indicating strong X-ray attenuation capability. To explore the X-ray response properties of the crystals, simple X-ray detector devices were fabricated by applying carbon–carbon (C–C) electrodes (0.9 mm^2) on the crystal surface, as illustrated in Fig. 3(b). The current–voltage (*I*–*V*) curves of (3AMPY)(MA)Pb_2Br_7 in the dark state are shown in Fig. 4(c), from which the volume resistivity of the crystals was determined to be 1.78 × 10^9 Ω cm. Such a high resistivity is essential for suppressing dark current, thereby achieving stable and high-performance X-ray detection. In addition to the improved X-ray attenuation, a high-performance detector must also facilitate efficient charge collection, which can be evaluated using the mobility–lifetime ($\mu\tau$) product. Furthermore, the $\mu\tau$ product of (3AMPY)(MA)Pb_2Br_7 is derived using the modified Hecht equation:[24]

$$I = \frac{I_0 \mu\tau}{d^2}\left[1 - \exp\left(\frac{-d^2}{\mu\tau V}\right)\right]$$

in which *d* is the electrode spacing, I_0 is the saturated photocurrent, *V* is the bias, and *I* is the photocurrent.

The $\mu\tau$ value of (3AMPY)(MA)Pb_2Br_7 was determined to be 9.3 × 10^{-4} cm^2 V^{-1} (in Fig. 3(d)), which is comparable to those of several published two-dimensional perovskites, such as (BDA)PbI_4 (4.43 × 10^{-4} cm^2 V^{-1}) and $(F\text{-}PEA)_2PbI_4$ (5.10 × 10^{-4} cm^2 V^{-1}).[24,25] We simultaneously grew pure 2D perovskite crystals of 3AMPYPbBr_4 using the same method and found their $\mu\tau$ value to be 1.02 × 10^{-4} cm^2 V^{-1} (in Fig. S1, ESI†). This indicates that the $\mu\tau$ value of (3AMPY)(MA)Pb_2Br_7 crystals is approximately ten times greater than that of 3AMPYPbBr_4. We believe this significant difference can be explained

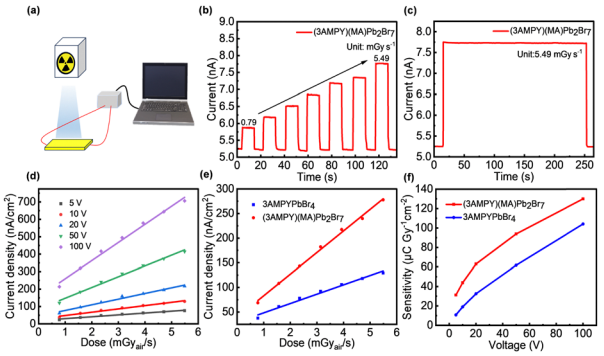

Fig. 4 (a) Schematic diagram of the X-ray test system. (b) Response curves at different X-ray dose rates. (c) X-ray response stability test. (d) Device sensitivity at different voltages. (e) Comparison of the sensitivity of two crystals at 10 V. (f) Comparison of the sensitivity of two crystals with voltage at different voltages.

structurally: the quasi-2D perovskite structure exhibits minimal variation in the spacing of the large organic A-site cation layers compared to the pure 2D perovskite. However, the presence of MA^+ increases the number of inorganic layers, thereby improving electron transport. Thus, the quasi-2D perovskite crystals of $(3AMPY)(MA)Pb_2Br_7$ have a higher $\mu\tau$ product.

Then, we built the X-ray detection system shown in Fig. 4(a) and characterized the X-ray detection performance of the devices described above. The *I–V* curve of $(3AMPY)(MA)Pb_2Br_7$ under X-rays demonstrates excellent X-ray responsiveness. As shown in Fig. 4(b), the photocurrent increases linearly with the X-ray dose rate at a 10 V bias, indicating a good photoresponse to X-rays. Fig. 4(c) shows the current–time (*IT*) curve of the device under a continuous X-ray pulse with a dose rate of 5.49 mGy s^{-1}, demonstrating that the single-crystal (SC) device exhibits a considerable and stable signal response. Sensitivity, which is the quantity of charge gathered per unit area under X-rays, is a crucial factor in assessing the response of X-ray devices. It may be computed using the formula below:

$$S = \frac{(J_P - J_d)}{D}$$

where D is the X-ray dosage rate, J_d and J_P are the current densities in the dark and under X-rays, respectively, and S is the sensitivity.[20] According to Fig. 4(d), the current density exhibits a linear correlation with the dose rate. By fitting the data, the crystals demonstrated a sensitivity of 43.86 μC Gy^{-1} cm^{-2} at a bias voltage of 10 V. Subsequent measurements of the sensitivity changes at different voltages indicated that sensitivity gradually increased with increasing voltage, reaching 129.86 μC Gy^{-1} cm^{-2} at 100 V. Finally, in Fig. 4(e) and (f), we also compare the performance difference in X-ray detection between this device and the device prepared from pure 2D perovskite $3AMPYPbBr_4$ crystals under the same conditions. The results show that the quasi-2D perovskite device exhibits a greater response to X-rays and improves the device sensitivity.

In summary, by leveraging the thermodynamics of chemical reactions and carefully adjusting the temperature of the environment at different stages of the mixed reaction system, we successfully regulated the reaction progress and obtained the desired final products. We successfully synthesized the large quasi-two-dimensional DJ halide perovskite $(3AMPY)(MA)Pb_2Br_7$ with a size of about 10 mm × 5 mm × 4 mm. Simple X-ray detectors based on $(3AMPY)(MA)Pb_2Br_7$ crystals were fabricated and tested, demonstrating excellent semiconductor properties, including a high resistivity of 1.78×10^9 Ω cm and a $\mu\tau$ product of 9.3×10^{-4} cm^2 V^{-1}. The devices exhibited outstanding detection performance with a dark current density of 5.6×10^{-8} A cm^{-2} V^{-1} and a sensitivity of 129.86 μC Gy^{-1} cm^{-2}. The excellent detection performance and stability position $(3AMPY)(MA)Pb_2Br_7$ as a promising candidate for X-ray detection. This work provides a universally applicable growth method for synthesizing large-scale, high quality quasi-2D perovskite single crystals, overcoming a long-standing bottleneck.

Data availability

The authors confirm that the data supporting the findings of this study are available within the article.

Conflicts of interest

The authors declare that they have no known competing financial interests or personal relationships that could have appeared to influence the work reported in this paper.

Notes and references

1 J. Androulakis, *et al.*, *Adv. Mater.*, 2011, **23**, 4163–4167.
2 J. Fan, *et al.*, *Adv. Funct. Mater.*, 2024, 2401017.
3 Y. Chen, *et al.*, *InfoMat*, 2024, **6**, e12596.
4 P. Jin, *et al.*, *Nat. Commun.*, 2023, **14**, 626.
5 T. Lyu and P. Dorenbos, *Appl. Phys. Rev.*, 2024, **11**, 011415.
6 X. Li, *et al.*, *Inorg. Chem.*, 2023, **62**, 7914–7920.
7 H. Wei, *et al.*, *Nat. Photonics*, 2016, **10**, 333–339.
8 W. Pan, *et al.*, *Adv. Mater.*, 2019, **31**, 1904405.
9 S. Tie, *et al.*, *Chem. Commun.*, 2023, **59**, 5016.
10 T. Lyu and P. Dorenbos, *Appl. Phys. Rev.*, 2024, **11**, 041417.
11 T. Zhang, C. Hu and S. Yang, *Small Methods*, 2019, **4**, 1900552.
12 Y. Liu, *et al.*, *Matter*, 2020, **3**, 180–196.
13 A. Wibowo, *et al.*, *Commun. Mater.*, 2023, **4**, 21.
14 Z. Xin, *et al.*, *Adv. Funct. Mater.*, 2024, **34**, 2402480.
15 J. Wang, *et al.*, *Chem. Commun.*, 2024, **60**, 3311.
16 B. Wang, *et al.*, *ACS Energy Lett.*, 2023, **8**, 4406–4413.
17 Q. Fan, *et al.*, *Adv. Funct. Mater.*, 2023, **34**, 2312395.
18 N. Zhou and H. Zhou, *Small Struct.*, 2022, **3**, 2100232.
19 Y. Zhang and N.-G. Park, *ACS Energy Lett.*, 2022, **7**, 757–765.
20 C. Ji, *et al.*, *Adv. Funct. Mater.*, 2019, **30**, 1905529.
21 K. Dong, *et al.*, *Adv. Mater.*, 2024, **36**, 2313889.
22 D. Liu, *et al.*, *J. Mater. Chem. A*, 2024, **12**, 12467–12474.
23 A. A. Zhumekenov, *et al.*, *J. Am. Chem. Soc.*, 2024, **146**, 6706–6720.
24 Q. Guan, *et al.*, *Small*, 2023, **20**, 2307908.
25 H. Li, *et al.*, *Adv. Mater.*, 2020, **32**, 2003790.

